Physiological Measurement

IPEM Institute of Physics and Engineering in Medicine

PAPER

A multi-scale and multi-domain heart sound feature-based machine learning model for ACC/AHA heart failure stage classification

To cite this article: Yineng Zheng *et al* 2022 *Physiol. Meas.* **43** 065002

IOP Publishing Physiol. Meas. 43 (2022) 065002 https://doi.org/10.1088/1361-6579/ac6d40

Physiological Measurement

IPEM Institute of Physics and Engineering in Medicine

RECEIVED
7 February 2022

REVISED
21 April 2022

ACCEPTED FOR PUBLICATION
5 May 2022

PUBLISHED
28 June 2022

PAPER

A multi-scale and multi-domain heart sound feature-based machine learning model for ACC/AHA heart failure stage classification

Yineng Zheng[1,2,3,*], **Xingming Guo**[4,*], **Yingying Wang**[5], **Jian Qin**[5] and **Fajin Lv**[1,2,3]

[1] Department of Radiology, The First Affiliated Hospital of Chongqing Medical University, Chongqing 400016, People's Republic of China
[2] State Key Laboratory of Ultrasound in Medicine and Engineering, Chongqing Medical University, Chongqing 400016, People's Republic of China
[3] Medical Data Science Academy, Chongqing Medical University, Chongqing 400016, People's Republic of China
[4] Key Laboratory of Biorheology Science and Technology, Ministry of Education, College of Bioengineering, Chongqing University, Chongqing 400044, People's Republic of China
[5] Department of Cardiology, The First Affiliated Hospital of Chongqing Medical University, Chongqing 400016, People's Republic of China
[*] Authors to whom any correspondence should be addressed.

E-mail: yinengzheng@cqmu.edu.cn **and** guoxm@cqu.edu.cn

Keywords: heart sounds, chronic heart failure, ACC/AHA heart failure stages, classification

Abstract

Objective. Heart sounds can reflect detrimental changes in cardiac mechanical activity that are common pathological characteristics of chronic heart failure (CHF). The ACC/AHA heart failure (HF) stage classification is essential for clinical decision-making and the management of CHF. Herein, a machine learning model that makes use of multi-scale and multi-domain heart sound features was proposed to provide an objective aid for ACC/AHA HF stage classification. *Approach.* A dataset containing phonocardiogram (PCG) signals from 275 subjects was obtained from two medical institutions and used in this study. Complementary ensemble empirical mode decomposition and tunable-Q wavelet transform were used to construct self-adaptive sub-sequences and multi-level sub-band signals for PCG signals. Time-domain, frequency-domain and nonlinear feature extraction were then applied to the original PCG signal, heart sound sub-sequences and sub-band signals to construct multi-scale and multi-domain heart sound features. The features selected via the least absolute shrinkage and selection operator were fed into a machine learning classifier for ACC/AHA HF stage classification. Finally, mainstream machine learning classifiers, including least-squares support vector machine (LS-SVM), deep belief network (DBN) and random forest (RF), were compared to determine the optimal model. *Main results*. The results showed that the LS-SVM, which utilized a combination of multi-scale and multi-domain features, achieved better classification performance than the DBN and RF using multi-scale or/and multi-domain features alone or together, with average sensitivity, specificity, and accuracy of 0.821, 0.955 and 0.820 on the testing set, respectively. *Significance.* PCG signal analysis provides efficient measurement information regarding CHF severity and is a promising noninvasive method for ACC/AHA HF stage classification.

1. Introduction

Chronic heart failure (CHF) is a multietiological disease that can occur when cardiac output is insufficient for satisfying the needs of the body, and is the predominant clinical presentation in the typical end-stage of multiple cardiovascular diseases. According to the American Heart Association/American College of Cardiology (ACC/AHA) guideline (Yancy *et al* 2017), CHF can be classified into four stages (stages A, B, C and D) ranging from developing heart failure (HF) without current or prior symptoms to advanced HF. The progression of CHF can result in irreversible structural or functional cardiac tissue impairment. Once symptoms develop, stage CHF is present and will never revert to stage B again (Ren *et al* 2020). Because early detection of CHF makes timely

intervention possible and delays the progression of CHF, in addition to be beneficial for improving long-term prognosis (Goldberg and Jessup 2006), it is necessary to develop a convenient screening approach for the early identification of CHF. Accurate classification of ACC/AHA HF stages plays an important role in clinical practice (Gong *et al* 2017), but current guidelines do not provide objective classification strategies for HF stages. Thus, development of a cost-effective approach that supports automatic HF stage classification is urgently needed for establishing a screening of CHF, evaluating prognosis, and guiding therapy in clinical cardiology.

Symptoms and signs of HF are neither sensitive nor specific in early stage, which makes the clinical diagnosis of HF staging difficult and challenging (Ammar *et al* 2007). Heart sounds are the direct result of cardiac mechanical events, and cardiac auscultation allows practitioners to evaluate cardiac conditions efficiently and provides primary diagnostic clues for evaluating cardiac condition prior to performing a special cardiac examination. However, the use of cardiac auscultation is limited by imprecise judgements and human error that may occur due to young clinicians' inexperience. A phonocardiogram (PCG) is a high-fidelity digital record of heart sound signal acquired using an electronic auscultation device on the chest. Advanced machine learning techniques have been recently employed as mainstream approaches for the computer-aided diagnosis of cardiovascular diseases based on meaningful feature extraction from PCG signals (Dwivedi *et al* 2018, Alfaras *et al* 2019, Das *et al* 2020, Li *et al* 2020a, 2020b). Recently, many studies have focused on the automatic recognition of abnormalities based on heart sound classification (Eslamizadeh and Barati 2017, Whitaker *et al* 2017, Zhang *et al* 2017, Yadav *et al* 2020). Some researchers have applied PCG characteristics to the identification of heart valvular diseases (Tang *et al* 2018, Cheng *et al* 2020). Moreover, several studies have used multi-modal feature fusion for the detection of coronary heart disease (Winther *et al* 2018, Li *et al* 2020a). In contrast, the number of studies in which heart sounds are used for the detection of CHF is relatively small. Heart sound analysis has been shown potential in the differential diagnosis of CHF and the classification of HF phenotypes (Zheng *et al* 2015, Liu *et al* 2019). To our knowledge, machine learning classifiers built on PCG features have not been used previously in ACC/AHA HF stage classification. Furthermore, the relationship between heart sound features and specific HF stages is unknown, and whether changes in heart sound features reflect the severity of CHF and how these changes are related to the progression of CHF are also unknown.

Heart sound feature extraction is the process of unveiling hidden characteristic information about a PCG signal in different domains, including time (Whitaker *et al* 2017), frequency (Khan *et al* 2020), time-frequency (Lee *et al* 1999), and nonlinear features (Saeedi *et al* 2021), all of which can reflect the information about cardiac structure and function. A study that applied PCG features to the identification of coronary artery disease could serve as an inspiration for the presentation of multi-domain feature analysis (Schmidt *et al* 2015). Complementary ensemble empirical mode decomposition (CEEMD) (Yeh *et al* 2010), as a fully data-driven technique, was designed to perform multi-scale decomposition of signals into their natural scale components. The tunable-Q wavelet transform (TQWT) is a powerful multi-scale resolution technique that is well suited for deeply understanding the complex features of biomedical signals (Selesnick 2011). Theoretically, the use of a combination of multi-domain and multi-scale feature analysis methodologies may potentially improve the classification performance of machine learning models. We hypothesized that combining multi-domain and multi-scale heart sound features could provide deep insight into the feature representations of heart sound aberrations that might occur in different stages of CHF and improve the recognition of the corresponding multifarious signal patterns using machine learning to substantially facilitate auxiliary ACC/AHA HF stage classification. Therefore, this paper proposed to use CEEMD and TQWT to construct self-adaptive heart sound sub-sequences and multi-level heart sound sub-band signals for multi-scale feature extraction, respectively. Feature selection was performed using the least absolute shrinkage and selection operator (LASSO), and the selected multi-scale and multi-domain features were fed into a machine learning classifier for ACC/AHA HF stage classification. Finally, mainstream machine learning classifiers such as least-squares support vector machine (LS-SVM), deep belief networks (DBN) and random forest (RF) were used and compared to determine the optimal model.

The remainder of this paper is organized as follows. Descriptions of the methods used in data acquisition, preprocessing, multi-scale and multi-domain feature extraction, feature selection and classification model construction are introduced in section 2. Section 3 provides a detailed presentation of the experimental results. Section 4 presents the relevant discussion. Finally, the conclusion and future directions are summarized in section 5.

2. Method and materials

The framework for this study is based on the development of a multi-scale and multi-domain heart sound feature-based machine learning model for ACC/AHA HF stage classification, as shown in figure 1.

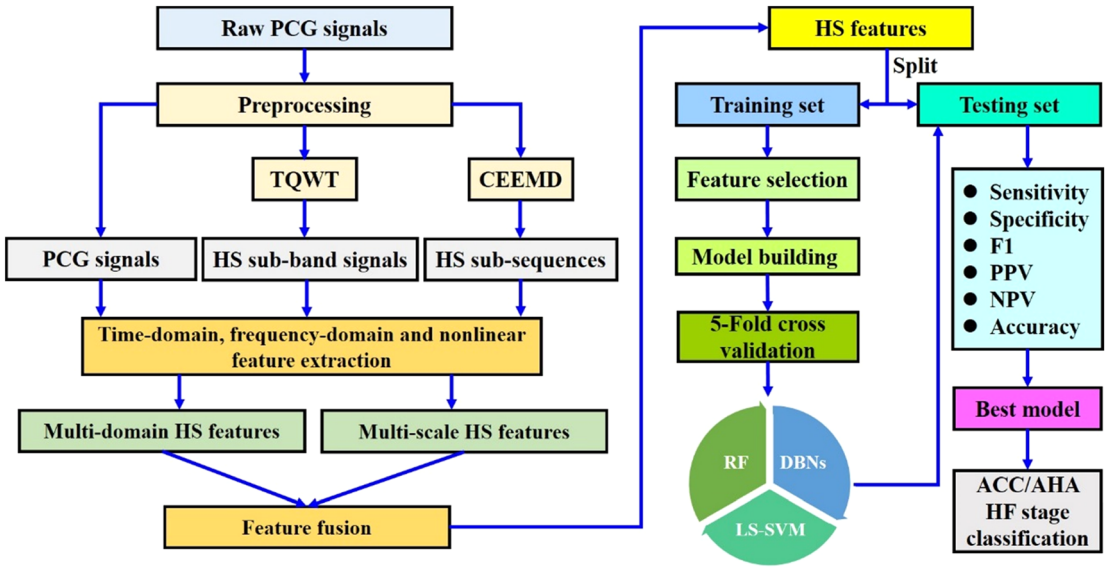

Figure 1. The framework of this study for ACC/AHA heart failure stage classification.

2.1. Study population

Heart sound data were obtained from two institutions such as the First Affiliated Hospital and the University-Town Hospital of Chongqing Medical University. Ethical approval for this study was obtained from both institutions. A total of 275 subjects, including 51 healthy volunteers and 224 patients with CHF, were recruited for this study. All the subjects were instructed to review and sign informed consent forms. The patients with CHF were confirmed and then grouped into four stages of HF such as stage A (at risk for HF), stage B (pre-HF), stage C (symptomatic HF) and stage D (advanced HF) by experienced cardiologists according to the most recently universal definition and classification of HF (Bozkurt *et al* 2021). Heart sound signal was recorded at the apex position of each subject in the resting state using a multichannel physiological measurement instrument (RM-6240BD, Chengdu Instrument Factory, China) with an electronic transducer (XJ102) at a sampling frequency of 8000 Hz. To enlarge the sample size for machine learning, each 5 min recording was cropped to 5 non-overlapping frame signals with a length of 20 s. Consequently, a total of 1375 samples were generated. The demographic information of the experimental data and the universal definition of HF stages are summarized in table 1.

2.2. Preprocessing

Before feature extraction, preprocessing was performed to obtain clean and normalized heart sound signals via the following sequence:

(1) Noise cancellation: A fourth-order adaptive finite impulse response notch filter was used for 50 Hz power line interference. The low-frequency noise and baseline drift were then removed by a high-pass Butterworth filter with a cut-off frequency of 10 Hz. Finally, multi-level singular value decomposition and compressed sensing were applied to remove white noise and environmental noise from the heart sound signals (Zheng *et al* 2017).

(2) Normalization: Z-score normalization was performed for each signal.

(3) Segmentation: An efficient and specialized hidden semi-Markov model segmentation algorithm was used to segment and crop each heart sound signal into non-overlapping frame signals (Springer *et al* 2015).

(4) Resampling: The frequency components of heart sounds range from 10 to 1000 Hz, and the sampling frequency was reset to 2000 Hz to reduce the computational complexity.

2.3. Self-adaptive heart sound sub-sequence construction

To perform the frequency-domain and nonlinear analysis of heart sound sub-sequences, CEEMD was used to decompose the input heart sound signals into several intrinsic mode function (IMF) components, and the IMF that showed the highest correlation with the original signal was then selected as the heart sound sub-sequence. CEEMD overcomes the disadvantages of incomplete decomposition derived from empirical mode

Table 1. Basic characteristics of the sample data.

Type	Universal definition	Number of subjects	Age (year)	Number of signals
Healthy subject	No cardiovascular diseases	51	47 (24–57)	255
HF Stage A	At high risk for HF but no structural heart disease or symptoms of HF	42	58 (42–69)	210
HF Stage B	Asymptomatic structural heart disease or abnormal cardiac function without symptoms or signs of HF	56	61 (48–72)	280
HF Stage C	Structural and/or functional cardiac abnormality with symptoms of HF	75	62 (56–75)	375
HF Stage D	Refractory HF with advanced symptoms that do not get better with treatment	51	64 (58–79)	255

decomposition by adding random Gaussian white noise to the original signals (Yeh *et al* 2010). To accomplish this, N pairs of positive and negative Gaussian white noise were added to the original heart sound signal as follows:

$$\begin{bmatrix} M_1 \\ M_2 \end{bmatrix} = \begin{bmatrix} 1 & 1 \\ 1 & -1 \end{bmatrix} \begin{bmatrix} S(n) \\ W(n) \end{bmatrix}, \tag{1}$$

where $W(n)$ denotes the Gaussian white noise, and M_1 and M_2 are the sums of the original signals with positive and negative Gaussian white noise, respectively.

CEEMD was applied to the target signal, and each signal yielded a set of IMF components; the ith component of the jth IMF is expressed as IMF_{ij}.

The results of each IMF were obtained after averaging the overall ensemble. This step can be formulated as:

$$\mathrm{IMF}_j(n) = \frac{1}{2N}\sum_{i=1}^{2N} \mathrm{IMF}_{ij}(n). \tag{2}$$

Hence, the final CEEMD result of $S(n)$ can be denoted as:

$$S(n) = \sum_{j=1}^{K} \mathrm{IMF}_j(n) + \mathrm{res}. \tag{3}$$

In this study, the standard deviation of the Gaussian white noise was specified as the standard deviation of the original signal multiplied by 0.2. Pearson's correlation analysis was used to evaluate the correlation between each IMF and the original signal, and IMFs with correlation coefficients greater than 0.2 were selected as heart sound sub-sequences. Herein, the first four IMFs (IMF1-4) were used to constitute the heart sound sub-sequences.

2.4. Multi-level heart sound sub-band signal construction

In this study, the utilization of heart sound sub-band features for HF stage classification was proposed. A crucial step in this process is the decomposition of a heart sound signal into multi-level sub-band signals using TQWT, which has the potential to aid in the analysis of oscillatory signals by tuning the Q-factor (Q), the redundancy factor (r) and the number of decomposition levels (J) (Selesnick 2011). The non-rational transfer functions are used to facilitate the implementation of TQWT filters in the frequency-domain. The multi-level TQWT decomposition can be achieved by applying two-channel filter banks consisting of low-pass and high-pass filters ($H_0(\omega)$ and $H_1(\omega)$) periodically to the low-pass sub-band signals, where ω is the angular frequency. Let us consider a heart sound signal $S(n)$ with a sampling rate f_s at the Jth level decomposition; the low-pass and high-pass sub-band signals, denoted by $a^J(n)$ and $d^J(n)$, respectively, are generated from low-pass and high-pass filters denoted by $H_0^{(J)}(\omega)$ and $H_1^{(J)}(\omega)$, followed by a low-pass scaling operation α and a high-pass scaling operation β, respectively. Figure 2 shows the equivalent systems of the TQWT decomposition and the Jth level decomposition of the input signal for the generation of the low-pass and high-pass sub-band signals. The frequency responses of the low-pass filter $H_0^{(J)}(\omega)$ and the high-pass filter $H_1^{(J)}(\omega)$ at the Jth level decomposition are given by

$$H_0^{(J)}(\omega) = \begin{cases} \prod_{m=0}^{J-1} H_0(\omega/\alpha^m), & |\omega| \leqslant \alpha^J\pi \\ 0, & \alpha^J\pi < |\omega| \leqslant \pi \end{cases} \tag{4}$$

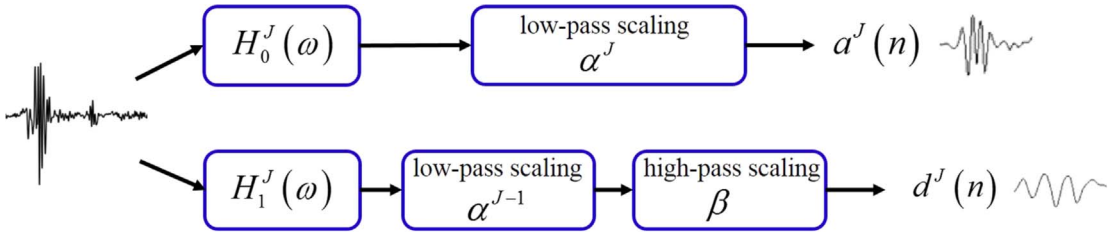

Figure 2. Equivalent systems for low-pass and high-pass sub-band signals.

$$H_1^{(J)}(\omega) = \begin{cases} H_1(\omega/\alpha^{J-1}) \prod_{m=0}^{J-2} H_0(\omega/\alpha^m), & (1-\beta)\alpha^{J-1}\pi \leqslant |\omega| \leqslant \alpha^{J-1}\pi \\ 0, & \omega \in [-\pi, \pi] \end{cases}, \tag{5}$$

where $J \in \mathbb{N}$.

$H_0(\omega)$ and $H_1(\omega)$ are defined in terms of $\theta(\omega)$, which is the frequency response of the Dabuchies filter (Li *et al* 2019) with two vanishing moments

$$H_0(\omega) = \theta\left(\frac{\omega + (\beta-1)\pi}{\alpha+\beta-1}\right), \ (1-\beta)\pi < |\omega| < \alpha\pi \tag{6}$$

$$H_1(\omega) = \theta\left(\frac{\alpha\pi - \omega}{\alpha+\beta-1}\right), \ (1-\beta)\pi < |\omega| < \alpha\pi \tag{7}$$

$$\theta(\omega) = \frac{1}{2}(1 + \cos(\omega))(2 - \cos(\omega))^{1/2}, \ |\omega| \leqslant \pi. \tag{8}$$

The reconstruction of input signal was achieved with the selected sub-bands by employing a filter bank analogous to that employed during the decomposition stage. In terms of α and β, the parameters r and Q are expressed as

$$r = \frac{\beta}{1-\alpha} \tag{9}$$

$$Q = \frac{2-\beta}{\beta}. \tag{10}$$

In the TQWT implementation, the Q-factor and r are pre-defined. Using these values, the scaling parameters α and β are determined by the following relations:

$$\alpha = 1 - \frac{\beta}{r} \tag{11}$$

$$\beta = \frac{2}{Q+1}. \tag{12}$$

The Q-factor controls the number of oscillations of the wavelet, and the redundancy factor regulates the overlapping of the frequency responses. In this study, Q-factor $= 2.4$ and $r = 3$ were used. After the 6th TQWT decomposition, the lowest frequency sub-band signal $a^6(n)$ and three high-pass sub-band signals $d^{4,5,6}(n)$ were selected as heart sound sub-band signals.

2.5. Time-domain features

The time-domain features of heart sounds are the quantitative representations of morphological heart sound waveform characteristics obtained by calculating the amplitudes, interval durations and amplitude or interval ratios of heart sound components. The amplitude of the first heart sound is associated with the rate of change in left ventricular pressure, which can represent the intensity of cardiac contractility, and the interval durations of cardiac mechanical activities are associated with coronary blood flow reserve. Therefore, heart sound time-domain features may be potentially helpful in the classification of HF stages for which the cardiac hemodynamic parameters differ. In this study, 6 time-domain features were calculated, and the details are given in table 2.

2.6. Multi-scale frequency-domain features

The frequency characteristics of heart sound signals potentially reflect the information about myocardial contraction, atrioventricular valve activity, and blood flow in the heart. The main frequencies of normal heart

Table 2. The detail of time-domain features of heart sounds.

Feature sign	Definition
S1/S2	The ratio of first heart sound amplitude to second heart sound amplitude
D/S	The ratio of diastolic duration to systolic duration
IntS1/D	The ratio of S1 interval duration to diastolic duration
IntS1/S	The ratio of S1 interval duration to systolic duration
IntS2/D	The ratio of S2 interval duration to diastolic duration
IntS2/S	The ratio of S2 interval duration to systolic duration

sounds range from 10 to 200 Hz, but a number of abnormal cardiac hemodynamic changes alter the frequency components of heart sounds. High-frequency heart sounds whose dominant frequencies are approximately 400–800 Hz are regarded as heart murmurs. Except for the investigation of frequency-domain features, CEEMD and TQWT decomposition were employed to construct the heart sound sub-sequences and sub-band signals that could represent multi-scale information in different frequency ranges. We first calculated the energy proportions of the low-frequency components of the heart sound signal below 200 Hz in total and then calculated the energy proportions of different heart sound sub-sequences and sub-band signals in the total signal using CEEMD and TQWT, respectively. These features were used to explore whether the spectral distributions of the frequency components of the heart sounds differed among patients at different stages of HF and whether they differed between patients with CHF and healthy subjects. In this study, 9 multi-scale frequency-domain features were proposed, and they are described in table 3.

2.7. Multi-scale nonlinear features

Heart sound signals are derived from cardiac mechanical activity; because the heart is a typical nonlinear system, the signals produced by its activity also have the properties of a nonlinear time series. Therefore, entropy-based complexity analysis and fractal geometry-based self-similarity analysis were employed to reflect the changes in the inherent characteristics that are correlated with nonlinear cardiac dynamics in patients in the different HF stages. 18 multi-scale nonlinear features are listed in table 4.

2.7.1. Entropy-based complexity analysis

The sample entropy (SE) is the improved algorithm derived from the approximate entropy (Lake *et al* 2002), and it offers a better measurement of entropy and is an efficient approach that reflects tiny changes in the complexity of time series data. Because entropy is related to the rate of production of energy or information within a system, the SE of heart sounds can be used to quantify the complexity of cardiac mechanical activity. It can be computed using the following statistical estimation formula:

$$SampEn(m,\ r,\ N) = -\ln\left(\frac{A_m(r)}{B_m(r)}\right), \tag{13}$$

where m and r represent the embedding dimension and the tolerance level, respectively. In our study, SE was applied to the original heart sound signals, sub-sequences and sub-sub-band signals. The tolerance level r was set to the 0.2-fold standard deviation of the sequence. The value of m was determined in terms of the Cao algorithm (Cao 1997).

2.7.2. Fractal geometry based self-similarity analysis

The multifractal spectrum measures deviations in the fractal structure, which is composed of small and large fluctuations within the time sequences (Falconer 1994). The multifractal spectrums of the original heart sound signals, heart sound sub-sequences and sub-band signals were calculated using the multifractal detrended fluctuation analysis (MF-DFA) approach, which gives the description of the variations and self-similarity within fractal structures at different time scales (Ihlen 2012). The MF-DFA computation was performed as shown below.

The fluctuation function can be described as follows:

$$F_q(s) \equiv \left\{\frac{1}{2N_s}\sum_{v=1}^{2N_s}[F^2(s,\ v)]^{\frac{q}{2}}\right\}^{\frac{1}{q}}, \tag{14}$$

Table 3. The detail of multi-scale frequency-domain features of heart sounds

Feature sign	Definition
LF_EF	The ratio of signal energy of heart sound below 200 Hz to that of the total signal
IMF1_EF	The ratio of signal energy of heart sound sub-sequence constructed by IMF1 to that of the total signal
IMF2_EF	The ratio of signal energy of heart sound sub-sequence constructed by IMF2 to that of the total signal
IMF3_EF	The ratio of signal energy of heart sound sub-sequence constructed by IMF3 to that of the total signal
IMF4_EF	The ratio of signal energy of heart sound sub-sequence constructed by IMF4 to that of the total signal
Sub1_EF	The ratio of signal energy of heart sound sub-band signal constructed by sub-band1 to that of the total signal
Sub2_EF	The ratio of signal energy of heart sound sub-band signal constructed by sub-band2 to that of the total signal
Sub3_EF	The ratio of signal energy of heart sound sub-band signal constructed by sub-band3 to that of the total signal
Sub4_EF	The ratio of signal energy of heart sound sub-band signal constructed by sub-band4 to that of the total signal

Table 4. The detail of multi-scale nonlinear features of heart sounds.

Feature sign	Definition
SampEn	Sample entropy of heart sound signal
IMF1_SampEn	Sample entropy of heart sound sub-sequence constructed by IMF1 after CEEMD
IMF2_SampEn	Sample entropy of heart sound sub-sequence constructed by IMF2 after CEEMD
IMF3_SampEn	Sample entropy of heart sound sub-sequence constructed by IMF3 after CEEMD
IMF4_SampEn	Sample entropy of heart sound sub-sequence constructed by IMF4 after CEEMD
Sub1_SampEn	Sample entropy of heart sound sub-band signal constructed by sub-band1 after TQWT
Sub2_SampEn	Sample entropy of heart sound sub-band signal constructed by sub-band2 after TQWT
Sub3_SampEn	Sample entropy of heart sound sub-band signal constructed by sub-band3 after TQWT
Sub4_SampEn	Sample entropy of heart sound sub-band signal constructed by sub-band4 after TQWT
MFPwidth	Width of multifractal spectrum of heart sound signal
IMF1_MFPwidth	Width of multifractal spectrum of heart sound sub-sequence constructed by IMF1 after CEEMD
IMF2_MFPwidth	Width of multifractal spectrum of heart sound sub-sequence constructed by IMF2 after CEEMD
IMF3_MFPwidth	Width of multifractal spectrum of heart sound sub-sequence constructed by IMF3 after CEEMD
IMF4_MFPwidth	Width of multifractal spectrum of heart sound sub-sequence constructed by IMF4 after CEEMD
Sub1_MFPwidth	Width of multifractal spectrum of heart sound sub-band signal constructed by sub-band1 after TQWT
Sub2_MFPwidth	Width of multifractal spectrum of heart sound sub-band signal constructed by sub-band2 after TQWT
Sub3_MFPwidth	Width of multifractal spectrum of heart sound sub-band signal constructed by sub-band3 after TQWT
Sub4_MFPwidth	Width of multifractal spectrum of heart sound sub-band signal constructed by sub-band4 after TQWT

where s indicates the scale size of each segment, N_s is the number of segments, and q represents a fluctuation parameter that makes it possible to analyse fluctuations of different magnitudes.

The power law function estimates the scaling characteristics of fluctuation functions by calculating the log–log graphs of $F_q(s)$ versus s for each value of q, as follows:

$$F_q(s) \propto s^{h(q)}, \tag{15}$$

where $h(q)$ is the generalized Hurst exponent. Finally, by applying the Legendre transform to $h(q)$, we can obtain the multifractal spectrum $f(\alpha) \propto \alpha$ (figure 3). Here, we employ the multifractal spectrum width (MFPwidth) as a nonlinear feature to quantify the multifractal nature of heart sound signals.

2.8. Feature selection

The LASSO was applied to feature selection (Yamada *et al* 2014). This operator applies L1 regularization process and shrinks some irrelevant feature coefficients to zero to make it possible to perform variable selection from the global features. Therefore, it helps increase the interpretability of the resulting machine learning model by removing irrelevant feature variables that are not associated with the response variables; in this way, overfitting is reduced. In this study, LASSO logistic regression was used for feature selection (Kang *et al* 2019), which imposes a fixed upper bound on the sum of the absolute values of the model parameters by combining the advantages of ridge regression and subset selection.

2.9. Machine learning model

The selected features were fed into a machine learning model for HF stage classification. This study compared the performance of three typical machine learning approaches and chose the first-rank approach for classification model construction.

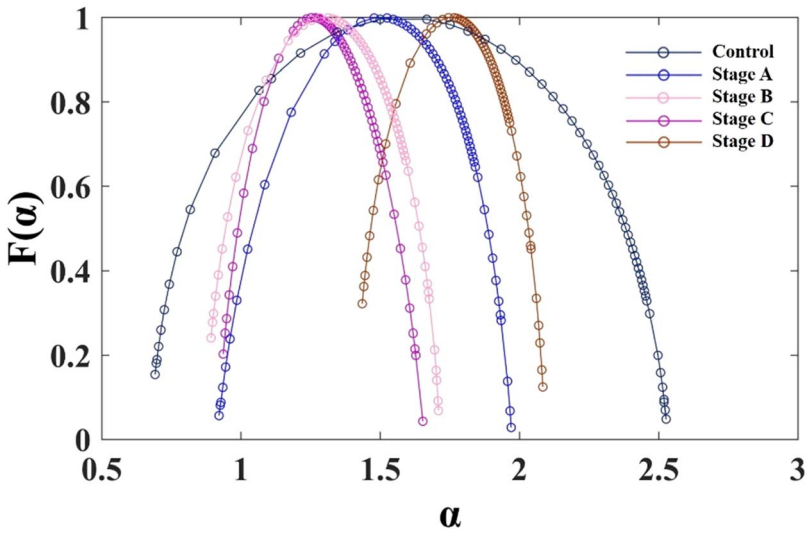

Figure 3. The illustration of multifractal spectrums for the heart sound signals from a healthy subject and from patients at different HF stages.

2.9.1. LS-SVM

The LS-SVM, which avoids solving a quadratic programming problem with high computational complexity by solving a group of linear equations, has emerged as a benchmark for solving small-sample classification problems in the biomedical field (Van Gestel *et al* 2004). In this study, the Gaussian radial basis function was employed as kernel function. During the calculation process, the values of kernel, penalty and tolerance parameters were chosen empirically to achieve the optimal system performance, as shown in table 5. Since the LS-SVM is a binary classifier, it solves multi-class classification problems by adopting one-against-all (OAA) and one-against-one strategies. In this study, the OAA strategy was utilized to classify five classes of heart sound signals.

2.9.2. Deep belief networks

A DBN, a probability generation model consisting of multiple hidden-layer neural networks, is constructed using multiple restricted Boltzmann machines (RBMs) (Mohamed *et al* 2011), In this model, each hidden layer of the subnetwork serves as the visible layer for the next layer. The DBN training process includes two stages: pretraining and fine-tuning. First, the RBM performs the layer-by-layer greedy learning algorithm to adjust the connection weight of the deep neural networks using contrastive divergence; in this process, maximum likelihood estimation is applied for updating of weights (Hinton 2012). Fine-tuning is then performed using a backpropagation (BP) algorithm to optimize the connection weights. The weight decay and sparsity penalty are used to overcome the problem of overfitting during the training phase. In this study, cross entropy was used as the cost function, and the softmax function was adopted at the top of the DBN model.

2.9.3. Random forest

Random forests are ensemble learning methods that operate by constructing a multitude of decision trees (Pal 2005). They use feature randomness and are usually trained with the bagging method when building several decision trees to try to create an uncorrelated forest of trees; the obtained results are then averaged. Each individual tree relies on a random sample of appropriate values and is a separate classifier. When training the nodes of each tree, the feature that is used is randomly selected from all features without replacement. Each tree in the RF algorithm yields its own classification selection and thus votes for that class; the overall output of the forest is the classification option with the most votes.

2.10. Performance evaluation

The overall dataset was categorized into different datasets via stratification and shuffling to ensure a similar original distribution across the datasets. The heart sound samples from one patient were not included in the different datasets. Overall, 30% of the data were selected randomly as an independent testing set, and the remaining data were used as the training set for model construction via 5-fold cross validation. Stratification into the training dataset was automatically performed without artificial intervention to avoid selection bias. A grid search approach was used to identify the optimal parameters for each classifier. To minimize the perturbation

Table 5. Hyperparameter optimization.

Classifier	Parameters
LS-SVM	Kernel function = RBF, Kernel parameter = 2, Penalty parameter = 80, Tolerance parameter = 0.001
DBN	Number of depth neural network layer = 3, Number of units per layer = 100, Learning rate = 0.01, Epochs = 40.
RF	Number of trees = 80, Max depth = 20, Seed = 1

problems encountered during feature selection and to examine the reproducibility of the experimental results, we randomly assigned the data to a training or testing cohort 10 times. Subsequently, the model was reconstructed and verified repeatedly. The classification performance of the models was evaluated using the area under the curve (AUC). Confusion matrix-related metrics such as sensitivity, specificity, positive predictive value (PPV), negative predictive value (NPV) and accuracy were also calculated. The detailed parameter settings for the used machine learning classifiers are listed in table 5.

2.11. Statistical analysis

The normality of all the continuous variables was assessed by the Shapiro–Wilk test to determine whether a parametric or a nonparametric test for comparison of variables should be performed. For the analysis of each heart sound feature, the Kruskal–Wallis test or one-way analysis of variance was performed, as appropriate, to compare the differences among different CHF stages and the control group, and post hoc analysis with Bonferroni correction was performed for both groups in the five-group case. The receiver operating characteristic curve was obtained for each model by varying the classification probability threshold. The differences among the AUC values yielded by the three models were assessed using the Delong test. All statistical analyses were conducted with R 3.6.0 (http://www.R-project.org). The level of statistical significance was set at a two-sided p value below 0.05.

3. Results

In our experiment, the preprocessing, feature extraction, and machine learning steps were implemented in MATLAB 2015b (MathWorks, Natick, MA, USA). The proposed procedures were performed on a computer workstation with a 3.70 GHz Intel Core i7-8700K CPU, a GeForce GTX 1080Ti (8G) GPU, 32 GB of RAM and a 64-bit Windows 10 operating system.

3.1. Multi-domain heart sound features among different HF stages

The time-domain features of heart sounds are presented in figures 4(A)–(F). Compared to those of healthy subjects, depressed D/S, S1/S2, IntS1/S, and IntS2/S were observed in the patients with CHF, and the values of these parameters decreased gradually with the progression of HF from stage A to stage D. IntS1/D and IntS2/D were found to be elevated in the patients with CHF, and they increased as HF gets worse. The variation trend of the low-frequency energy fraction (LF_EF) of heart sounds from individuals with the healthy cardiac condition to advanced HF is shown in figure 4(G). The LF_EF of heart sounds decreased as HF worsened. The nonlinear analysis showed that the SE and multifractal spectrum width ($\Delta\alpha$) of heart sounds were significantly higher in the healthy group than in the CHF group ($P = 0.015$ and 0.023, respectively, figures 4(H)–(I)). The SE and $\Delta\alpha$ of heart sound signals have similar decreasing tendency with the progression of CHF, and they manifest the greater values in stage A while show the smaller values in stage D. In the early stage of CHF (stages A or B), D/S, S1/S2, IntS1/S, IntS2/S, LF_EF, SE and $\Delta\alpha$ were found to be significantly higher than those in the advanced stage of CHF (stage C or D) (all adjusted $P < 0.05$). There were no significant differences between stages A and B in any of these parameters except for LF_EF and $\Delta\alpha$ (adjusted $P = 0.029$ and 0.008, respectively).

3.2. Multi-scale heart sound features among different HF stages

The multi-scale frequency, complexity and self-similarity characteristics of the heart sound signals decomposed from CEEMD and TQWT were explored. The energy fractions of IMF1 and IMF2 decreased, while those of IMF3 and IMF4 increased from HF stages A to D, and the similar trend was found for the sub-band signals (table 6). This indicated that the energy fraction of the heart sound signals in the early stage of CHF was mainly concentrated in the low-frequency range (70–140 Hz), and the high-frequency components of the heart sound signals tended to increase when CHF progressed to the end stage. The multi-scale SE and $\Delta\alpha$ in each heart sound sub-sequence and sub-band signal tended to decrease as the HF worsened from stages A to D, as shown in figures 5 and 6. The SE and $\Delta\alpha$ of sub-sequences and sub-band signals display smaller values in the advanced stage of CHF than those in the early stage.

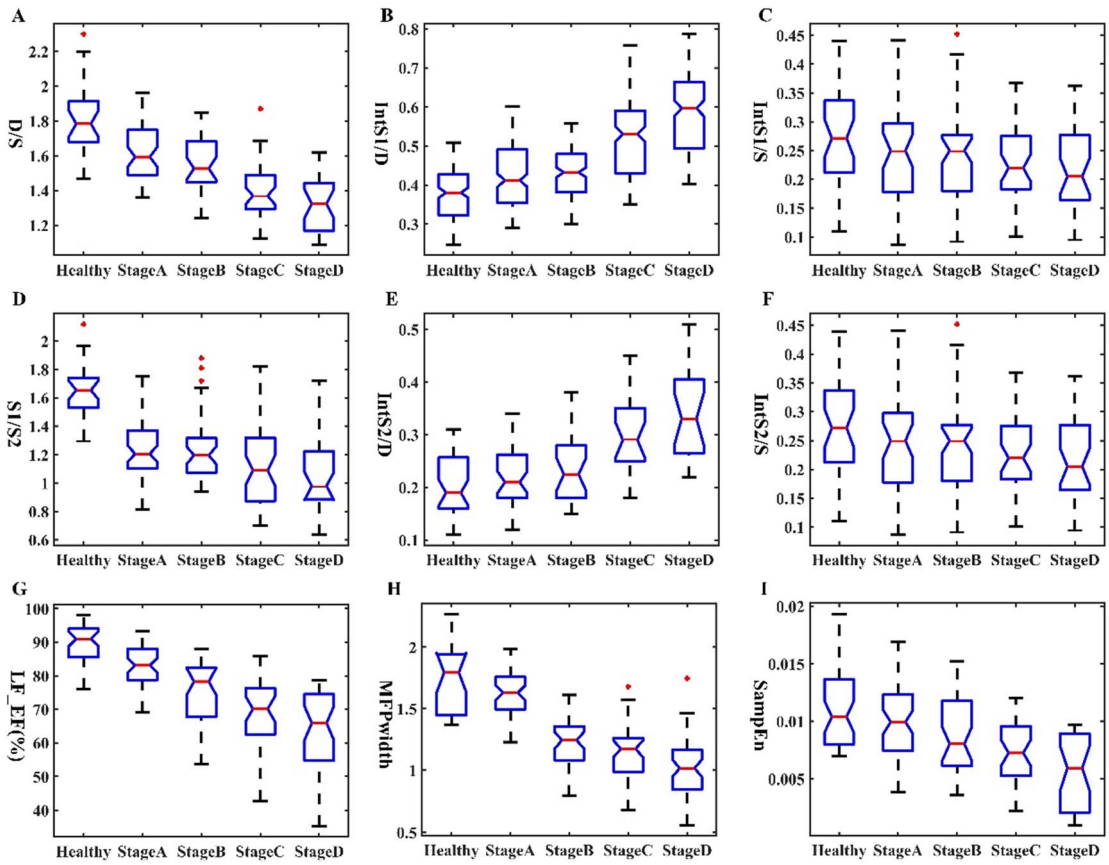

Figure 4. Multi-domain features of heart sound signals. (A) D/S, (B) IntS1/D, (C) IntS1/S, (D)S1/S2, (E) IntS2/D, (F) IntS2/S, (G) LF_EF, (H) MFPwidth, and (I) SampEn.

Table 6. The signal energy fractions of heart sound sub-sequences and sub-band signals.

		Control ($N = 255$)	Stage A ($N = 210$)	Stage B ($N = 280$)	Stage C ($N = 375$)	Stage D ($N = 255$)
Sub-sequences	IMF1_EF(%)	6.42 ± 0.53	3.47 ± 0.15	3.82 ± 0.49	3.14 ± 0.58	2.25 ± 0.54
	IMF2_EF(%)	41.52 ± 6.151	37.19 ± 3.78	35.75 ± 4.81	31.17 ± 4.78	28.92 ± 5.69
	IMF3_EF(%)	23.62 ± 4.98	24.82 ± 3.49	25.39 ± 4.68	26.50 ± 3.98	25.54 ± 7.43
	IMF4_EF(%)	10.12 ± 2.11	14.13 ± 2.86	16.34 ± 3.14	17.55 ± 3.62	19.96 ± 3.79
Sub-band signals	Sub1_EF(%)	5.87 ± 0.59	3.74 ± 0.36	3.45 ± 0.42	2.92 ± 0.51	2.47 ± 0.65
	Sub2_EF(%)	37.82 ± 5.47	35.59 ± 4.18	33.58 ± 5.31	31.61 ± 4.68	29.12 ± 6.59
	Sub3_EF(%)	23.67 ± 5.18	24.72 ± 4.69	26.31 ± 7.68	28.50 ± 5.98	29.56 ± 7.49
	Sub4_EF(%)	10.51 ± 24.12	12.12 ± 3.69	15.91 ± 4.14	17.50 ± 4.59	18.56 ± 4.08

3.3. Comparison of the classification performance of different machine learning-based HF stage classifiers

To determine the most appropriate model for the classification of HF stages, three representative machine learning classifiers such as LS-SVM, RF and DBN were used to automatically classify HF into four stages. The optimized hyperparameters of the three machine learning classifiers are listed in table 5; they were obtained via a grid search approach performed during the training process. The classification results of these three models on the training, validation, and testing sets are illustrated by the confusion matrices shown in figure 7. Table 7 presents the performance of the LS-SVM model in terms of automated HF stage classification, where each metric was calculated by averaging the results obtained in the 10 different runs completed for the 10 random splits of the heart sound data. The LS-SVM achieved an accuracy of 0.820 (95% CI: 0.734–0.925) and outperformed both the RF with an accuracy of 0.795 (95% CI: 0.687–0.902) and the DBN with an accuracy of 0.743 (95% CI: 0.625–0.871) on the HF stage classification task, which had sensitivity values ranging from 0.806 to 0.841 and specificity values ranging from 0.939 to 0.975 for the five classes of heart sounds.

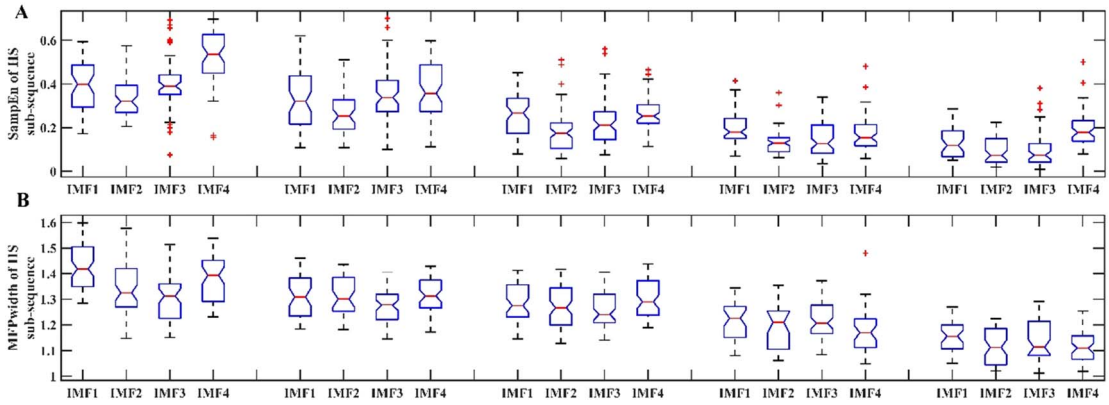

Figure 5. Multi-scale features of heart sound sub-sequences, (A) multi-scale multifractal spectrum width and (B) sample entropy. From left to right: healthy, stages A, B, C and D.

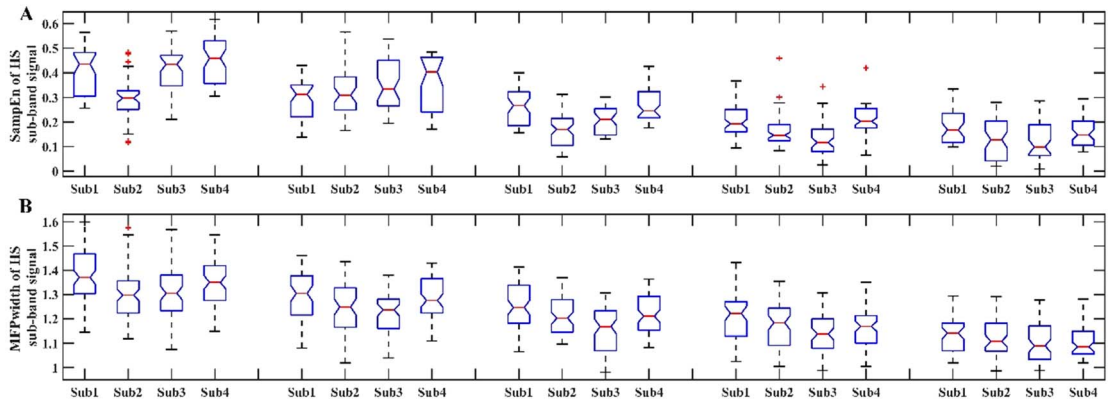

Figure 6. Multi-scale features of heart sound sub-band signals, (A) multi-scale multifractal spectrum width and (B) sample entropy. From left to right: healthy, stages A, B, C and D.

3.4. Use of a combination of multi-scale and multi-domain heart sound features

The multi-domain features extracted from the original PCG signals, the multi-scale features extracted from the heart sound sub-sequences and sub-band signals decomposed from the PCG signals, and a combination of both were fed into the LS-SVM model to obtain the corresponding classification results. As shown in figure 8, when the multi-scale features were used, the classification performance of the model was better than that achieved using the multi-domain features alone. The best result was obtained by using the combined features, and the accuracy increased from 0.741 to 0.820.

4. Discussion

In this study, we explored the changes in the time-domain, frequency-domain and nonlinear features of PCG signals along with the progression of HF and constructed an LS-SVM based machine learning model for the classification of HF stages using multi-scale and multi-domain heart sound features. Favourable classification performance was achieved in that the accuracy reached 0.871 (95% CI: 0.814–0.968) on the training set, 0.836 (95% CI: 0.768–0.914) on the validation set and 0.820 (95% CI: 0.734–0.925) on the testing set. Machine learning models that routinely combine clinical variables (Su *et al* 2014) or ECG features (Li *et al* 2019) have the potential to classify HF stages when varying degrees of cardiac mechanical dysfunction were detected. Since heart sounds are the acoustic vibrations that are produced during the mechanical processes of the cardiac cycle, they can be used for heart abnormality monitoring. Furthermore, PCG is noninvasive, resulting in convenience and time savings. When combined with machine learning, this technique has the potential to serve as a cost-effective auxiliary screening tool for HF stage classification and may offer a novel screening strategy for the patients who are at high risk of CHF or in its early stage.

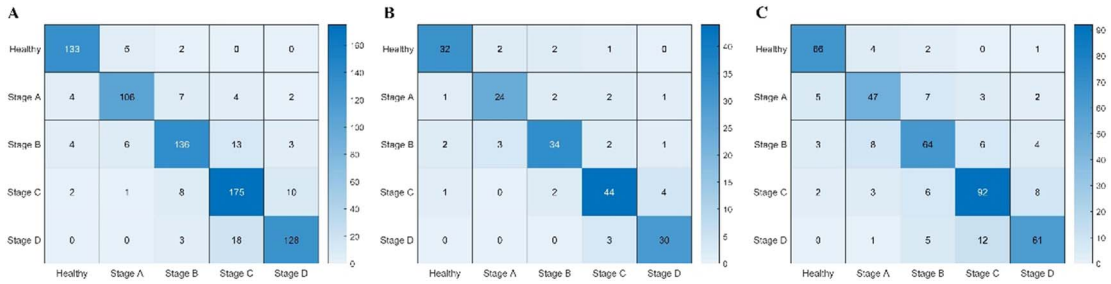

Figure 7. Confusion matrix for the classification of ACC/AHA heart failure stages using LS-SVM on the (A) training, (B) validation and (C) testing sets.

Table 7. The performance for ACC/AHA HF stage classification using LS-SVM on the training, validation and testing sets.

		Sensitivity	Specificity	F1	PPV	NPV	Accuracy
Training set	Control	0.910 ± 0.035	0.983 ± 0.034	0.916 ± 0.044	0.924 ± 0.064	0.980 ± 0.069	0.871 (95% CI: 0.814–0.968)
	A	0.876 ± 0.023	0.965 ± 0.028	0.847 ± 0.062	0.820 ± 0.071	0.977 ± 0.057	
	B	0.850 ± 0.041	0.957 ± 0.053	0.842 ± 0.028	0.834 ± 0.059	0.962 ± 0.052	
	C	0.845 ± 0.052	0.965 ± 0.047	0.871 ± 0.036	0.900 ± 0.073	0.943 ± 0.069	
	D	0.891 ± 0.043	0.969 ± 0.062	0.880 ± 0.041	0.869 ± 0.069	0.975 ± 0.061	
Validation set	Control	0.901 ± 0.039	0.952 ± 0.030	0.883 ± 0.059	0.888 ± 0.069	0.972 ± 0.083	0.836 (95% CI: 0.768–0.914)
	A	0.877 ± 0.028	0.948 ± 0.087	0.831 ± 0.038	0.802 ± 0.074	0.975 ± 0.092	
	B	0.830 ± 0.053	0.913 ± 0.049	0.792 ± 0.047	0.785 ± 0.058	0.947 ± 0.074	
	C	0.857 ± 0.047	0.923 ± 0.063	0.840 ± 0.075	0.843 ± 0.036	0.941 ± 0.067	
	D	0.828 ± 0.019	0.955 ± 0.062	0.839 ± 0.082	0.869 ± 0.047	0.957 ± 0.056	
Testing set	Control	0.841 ± 0.035	0.975 ± 0.048	0.861 ± 0.046	0.885 ± 0.019	0.962 ± 0.074	0.820 (95% CI: 0.734–0.925)
	A	0.826 ± 0.028	0.958 ± 0.065	0.802 ± 0.074	0.779 ± 0.028	0.967 ± 0.068	
	B	0.826 ± 0.057	0.939 ± 0.069	0.800 ± 0.071	0.776 ± 0.093	0.953 ± 0.065	
	C	0.806 ± 0.062	0.946 ± 0.074	0.828 ± 0.066	0.852 ± 0.074	0.928 ± 0.059	
	D	0.807 ± 0.049	0.955 ± 0.057	0.805 ± 0.057	0.803 ± 0.038	0.956 ± 0.083	

Studies of the relationship between heart sounds and cardiac contractility have inspired a new field of research in which cardiac inotropic analysis is used as an approach to detect and measure CHF (Xiao *et al* 2000, Shah and Michaels 2006, Tang *et al* 2017, Thakur *et al* 2017). We have previously proven the effectiveness of a heart sound-based machine learning model for differentiating between CHF and healthy people (Zheng *et al* 2015), and for the identification of HF subtypes such as HF with reduced ejection fraction (HFrEF) and HF with preserved ejection fraction (HFpEF) (Gao *et al* 2020). However, to our knowledge, no previous study has sought to quantitatively classify the ACC/AHA HF stages using heart sounds, specifically in terms of utilizing multi-scale and multi-domain heart sound features. In the present work, we moved forward to first investigate the variation in heart sound features along with the progression of HF from stage A to stage D and then constructed a multi-scale and multi-domain heart sound feature-based computer-aided diagnosis model for HF stage classification using machine learning.

Previous studies have shown that D/S can be used to noninvasively assess cardiac reserve (Cheng *et al* 2021). Depressed D/S was observed as CHF progressed through the four stages, which are termed stages A to D. This is because of the abnormal prolongation of the systolic duration or the shortening of the diastolic duration caused by compromised cardiac filling and function abnormality when CHF occurs (Xu *et al* 2018). This finding is also in accordance with the evidence that the most important aspect of cardiac dysfunction in HF patients is not the depressed cardiac performance observed in the basal resting state but rather the loss of cardiac reserve (Tan 1986). HF represents an impairment and failure of cardiac contractility and states that may result in systolic dysfunction as well as a low ejection fraction (Bloom *et al* 2017). Many studies have shown that HF can cause diminished cardiomyocyte contractility at the cellular level, which is manifested as decreased cardiac contractility in the patients with CHF (Norman *et al* 2011, Borlaug 2014). In addition, the strength of heart sounds has been shown to be related to the rate of change of left ventricular pressure and cardiac contractility (Hansen *et al* 1989, Tang *et al* 2013). This can explain the gradual decrease in S1/S2 with the progression of CHF.

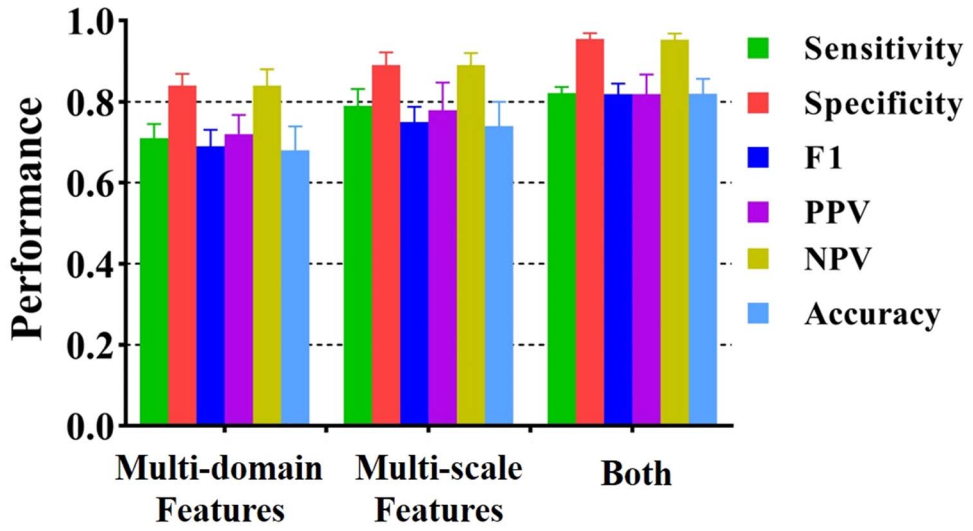

Figure 8. The average performance of LS-SVM model using multi-domain heart sound features, multi-scale heart sound features or a combination of both on the testing set. The sensitivity, specificity, F1, PPV and NPV and accuracy were calculated by the average of those values in different groups on the testing set where each metric was calculated by averaging the results obtained in the 10 different runs.

We found that the signal energy of the low-frequency components of heart sounds decreased as HF worsened. Since most of the energy in normal heart sound signals is concentrated in the low-frequency spectrum between 10 and 150 Hz (Safara *et al* 2013), an increase in the high-frequency components of heart sound signals indicates the occurrence of heart murmurs (Bozkurt *et al* 2018) that result from the impairment of the cardiac structure, such as aortic insufficiency and mitral regurgitation (Choi *et al* 2011), when HF progresses significantly. The decreases in the entropy and MFPwidth indicate that the complexity and self-similarity of the heart sound signals have decreased, respectively (Zheng and Guo 2017), and this suggests that decreased chaotic characteristics in cardiac mechanical activity can be observed. This is consistent with the changes in cardiac electrophysiological signals, such as electrocardiogram (ECG) signals (Turcott and Teich 1996, Jahmunah *et al* 2019).

In this study, a novel exploration of the changes that occur in the multi-scale information of heart sound signals as HF progressed from stages A to D was presented. We used CEEMD and TQWT to generate heart sound sub-sequences and sub-band signals with different frequency components and explored the changes in frequency, entropy and multifractal characteristics of those as HF progressed from stage A to stage D. The results indicate that the changes in multi-scale features obtained from heart sound sub-sequences and sub-band signals occur before those in conventional features when HF are detectable. The classification of multi-scale and multi-domain heart sound features therefore has the potential to facilitate early detection of subclinical CHF (stages A and B) and to provide information that can help physicians in their clinical decision-making regarding the initiation of direct and indirect treatment interventions.

The use of heart sound classification in the noninvasive diagnosis of cardiac diseases such as coronary heart disease (Liu *et al* 2021, Winther *et al* 2021) and congenital heart disease (Kui *et al* 2021, Lv *et al* 2021) has been widely explored. Focusing on the application of heart sound analysis for CHF has been shown to be efficient in terms of distinguishing healthy individuals from the patients with CHF and differentiating between HFpEF and HFrEF (Zheng *et al* 2015, Liu *et al* 2019). In contrast to those studies, we proposed to extract multi-scale heart sound features using CEEMD and TQWT and combining those features with other multi-domain heart sound features to construct an LS-SVM based machine learning model for ACC/AHA HF stage classification.

This study also has several limitations. First, it was a prospective study with a relatively small study cohort, and future studies should collect external validation data from different centres to enhance the generalization of the constructed machine learning model. Second, the clinical application of the proposed approach should be further validated using larger prospective studies with multicentric data. Third, although the heart is an electromechanical pump, heart sounds provide information on cardiac mechanical activity but not electrophysiological information, and therefore, the use of multi-modal cardiac physiological signals such as a combination of heart sound and ECG signals should be considered as a way of obtaining more comprehensive information on the global heart system. Fourth, a subgroup analysis should be performed.

5. Conclusion

This study demonstrates that heart sound signals represent a valuable source of information regarding the severity of CHF and the heart sound features change as CHF progresses. The LS-SVM based machine learning model using a combination of multi-scale and multi-domain heart sound features described in this work can be used as a potentially noninvasive method for ACC/AHA HF stage classification and may offer a promising and feasible way to improve clinical management and therapeutic decisions on the patients with CHF.

Funding

This study was supported by the National Natural Science Foundation of China (No. 31800823 and No. 31870980), the Natural Science Foundation of Chongqing (cstc2019jcyj-msxmX0395), Joint project of Chongqing Health Commission and Science and Technology Bureau (2022QNXM015), and Intelligent Medicine Research Project of Chongqing Medical University (ZHYX202102).

Conflict of interest statement

The authors declare no conflict of interest.

ORCID iDs

Yineng Zheng https://orcid.org/0000-0003-1698-6399
Xingming Guo https://orcid.org/0000-0003-3872-0866

References

Alfaras M, Soriano M C and Ortín S 2019 A fast machine learning model for ECG-based heartbeat classification and arrhythmia detection *Front. Phys.* **7** 103

Ammar K A, Jacobsen S J, Mahoney D W, Kors J A, Redfield M M, Burnett J C Jr and Rodeheffer R J 2007 Prevalence and prognostic significance of heart failure stages: application of the American College of Cardiology/American heart association heart failure staging criteria in the community *Circulation* **115** 1563–70

Bloom M W, Greenberg B, Jaarsma T, Januzzi J L, Lam C S, Maggioni A P, Trochu J-N and Butler J 2017 Heart failure with reduced ejection fraction *Nat. Rev. Dis. Primers* **3** 1–19

Borlaug B A 2014 The pathophysiology of heart failure with preserved ejection fraction *Nat. Rev. Cardiol.* **11** 507–15

Bozkurt B, Coats A J, Tsutsui H, Abdelhamid C M, Adamopoulos S, Albert N, Anker S D, Atherton J, Böhm M and Butler J 2021 Universal definition and classification of heart failure: a report of the heart failure Society of America, heart failure association of the European society of cardiology, Japanese heart failure society and writing committee of the universal definition of heart failure: endorsed by the Canadian heart failure society, heart failure association of India, cardiac society of Australia and New Zealand, and Chinese heart failure association *Eur. J. Heart Fail.* **23** 352–80

Bozkurt B, Germanakis I and Stylianou Y 2018 A study of time-frequency features for CNN-based automatic heart sound classification for pathology detection *Comput. Biol. Med.* **100** 132–43

Cao L 1997 Practical method for determining the minimum embedding dimension of a scalar time series *Physica D* **110** 43–50

Cheng L, Liao K, Wang Y, Lv F, Guo X, Zheng Y and Qin J 2021 Study of the correlation between the ratio of diastolic to systolic durations and echocardiography measurements and its application to the classification of heart failure phenotypes *Int. J. General Med.* **14** 5493–503

Cheng X, Wang P and She C 2020 Biometric identification method for heart sound based on multimodal multiscale dispersion entropy *Entropy* **22** 238

Choi S, Shin Y and Park H-K 2011 Selection of wavelet packet measures for insufficiency murmur identification *Expert Syst. Appl.* **38** 4264–71

Das S, Pal S and Mitra M 2020 Acoustic feature based unsupervised approach of heart sound event detection *Comput. Biol. Med.* **126** 103990

Dwivedi A K, Imtiaz S A and Rodriguez-Villegas E 2018 Algorithms for automatic analysis and classification of heart sounds–a systematic review *IEEE Access* **7** 8316–45

Eslamizadeh G and Barati R 2017 Heart murmur detection based on wavelet transformation and a synergy between artificial neural network and modified neighbor annealing methods *Artif. Intell. Med.* **78** 23–40

Falconer K J 1994 The multifractal spectrum of statistically self-similar measures *J. Theor. Probab.* **7** 681–702

Gao S, Zheng Y and Guo X 2020 Gated recurrent unit-based heart sound analysis for heart failure screening *Biomed. Eng. Online* **19** 1–17

Goldberg L R and Jessup M 2006 Stage B heart failure: management of asymptomatic left ventricular systolic dysfunction *Circulation* **113** 2851–60

Gong F F, Campbell D J and Prior D L 2017 Noninvasive cardiac imaging and the prediction of heart failure progression in preclinical stage A/B subjects *JACC: Cardiovascular Imaging* **10** 1504–19

Hansen P B, Luisada A A, Miletich D J and Albrecht R F 1989 Phonocardiography as a monitor of cardiac performance during anesthesia *Anesthesia Analgesia* **68** 385–7

Hinton G E 2012 A practical guide to training restricted Boltzmann machines *Neural Networks: Tricks of the Trade* (Berlin: Springer) pp 599–619

Ihlen E A F E 2012 Introduction to multifractal detrended fluctuation analysis in Matlab *Front. Physiol.* **3** 141
Jahmunah V, Oh S L, Wei J K E, Ciaccio E J, Chua K, San T R and Acharya U R 2019 Computer-aided diagnosis of congestive heart failure using ecg signals—a review *Physica Med.* **62** 95–104
Kang C, Huo Y, Xin L, Tian B and Yu B 2019 Feature selection and tumor classification for microarray data using relaxed Lasso and generalized multi-class support vector machine *J. Theor. Biol.* **463** 77–91
Khan F A, Abid A and Khan M S 2020 Automatic heart sound classification from segmented/unsegmented phonocardiogram signals using time and frequency features *Physiol. Meas.* **41** 055006
Kui H, Pan J, Zong R, Yang H and Wang W 2021 Heart sound classification based on log Mel-frequency spectral coefficients features and convolutional neural networks *Biomed. Signal Process. Control* **69** 102893
Lake D E, Richman J S, Griffin M P and Moorman J R 2002 Sample entropy analysis of neonatal heart rate variability *Am. J. Physiol.-Regulatory, Integrative Comparative Physiol.* **283** R789–97
Lee J J, Lee S M, Kim I Y, Min H K and Hong S H 1999 Comparison between short time Fourier and wavelet transform for feature extraction of heart sound *Proc. IEEE. IEEE Region 10 Conf. TENCON 99.'Multimedia Technology for Asia-Pacific Information Infrastructure'(Cat. No. 99CH37030)* (IEEE) pp 1547–50
Li D, Li X, Zhao J and Bai X 2019 Automatic staging model of heart failure based on deep learning *Biomed. Signal Process. Control* **52** 77–83
Li H, Wang X, Liu C, Zeng Q, Zheng Y, Chu X, Yao L, Wang J, Jiao Y and Karmakar C 2020a A fusion framework based on multi-domain features and deep learning features of phonocardiogram for coronary artery disease detection *Comput. Biol. Med.* **120** 103733
Li S, Li F, Tang S and Xiong W 2020b A review of computer-aided heart sound detection techniques *BioMed research international* **2020** 5846191
Liu T, Li P, Liu Y, Zhang H, Li Y, Jiao Y, Liu C, Karmakar C, Liang X and Ren M 2021 Detection of coronary artery disease using multi-domain feature fusion of multi-channel heart sound signals *Entropy* **23** 642
Liu Y, Guo X and Zheng Y 2019 An automatic approach using ELM classifier for HFpEF identification based on heart sound characteristics *J. Med. Syst.* **43** 1–8
Lv J, Dong B, Lei H, Shi G, Wang H, Zhu F, Wen C, Zhang Q, Fu L and Gu X 2021 Artificial intelligence-assisted auscultation in detecting congenital heart disease *Eur. Heart J.-Digital Health* **2** 119–24
Mohamed A-R, Dahl G E and Hinton G 2011 Acoustic modeling using deep belief networks *IEEE Trans. Audio Speech Lang. Process.* **20** 14–22
Norman H S, Oujiri J, Larue S J, Chapman C B, Margulies K B and Sweitzer N K 2011 Decreased cardiac functional reserve in heart failure with preserved systolic function *J. Cardiac Failure* **17** 301–8
Pal M 2005 Random forest classifier for remote sensing classification *Int. J. Remote Sens.* **26** 217–22
Ren Q W, Li Xl, Fang J, Chen Y, Wu M Z, Yu Y J, Liao Sg, Tse H F and Yiu K H 2020 The prevalence, predictors, and prognosis of tricuspid regurgitation in stage B and C heart failure with preserved ejection fraction *ESC Heart Failure* **7** 4051–60
Saeedi A, Moridani M K and Azizi A 2021 An innovative method for cardiovascular disease detection based on nonlinear geometric features and feature reduction combination *Intelligent Decision Technol.* **15** 45–57
Safara F, Doraisamy S, Azman A, Jantan A and Ramaiah A R A 2013 Multi-level basis selection of wavelet packet decomposition tree for heart sound classification *Comput. Biol. Med.* **43** 141407–14
Schmidt S E, Holst-Hansen C, Hansen J, Toft E and Struijk J J 2015 Acoustic features for the identification of coronary artery disease *IEEE Trans. Biomed. Eng.* **62** 2611–9
Selesnick I W 2011 Wavelet transform with tunable *Q*-factor *IEEE Trans. Signal Process.* **59** 3560–75
Shah S J and Michaels A D 2006 Hemodynamic correlates of the third heart sound and systolic time intervals *Congestive Heart Failure* **12** 8–13
Springer D B, Tarassenko L and Clifford G D 2015 Logistic regression-HSMM-based heart sound segmentation *IEEE Trans. Biomed. Eng.* **63** 822–32
Su F, Zhang S, Chen N, Wang J, Yao J, Tang J, Wu W and Chen D 2014 A heart failure staging model based on machine learning classification algorithms *Chin. J. Tissue Eng. Res.* **18** 7938–42
Tan L 1986 Cardiac pumping capability and prognosis in heart failure *Lancet* **328** 1136360
Tang H, Jiang Y, Li T and Wang X 2018 Identification of pulmonary hypertension using entropy measure analysis of heart sound signal *Entropy* **20** 389
Tang H, Ruan C, Qiu T, Park Y and Xiao S 2013 Reinvestigation of the relationship between the amplitude of the first heart sound to cardiac dynamics *Physiol. Rep.* **1** e00053
Tang H, Zhang J, Chen H, Mondal A and Park Y 2017 A non-invasive approach to investigation of ventricular blood pressure using cardiac sound features *Physiol. Meas.* **38** 289
Thakur P H, An Q, Swanson L, Zhang Y and Gardner R S 2017 Haemodynamic monitoring of cardiac status using heart sounds from an implanted cardiac device *ESC Heart Failure* **4** 605–13
Turcott R G and Teich M C 1996 Fractal character of the electrocardiogram: distinguishing heart-failure and normal patients *Ann. Biomed. Eng.* **24** 269–93
Van Gestel T, Suykens J A, Baesens B, Viaene S, Vanthienen J, Dedene G, De Moor B and Vandewalle J 2004 Benchmarking least squares support vector machine classifiers *Mach. Learn.* **54** 5–32
Whitaker B M, Suresha P B, Liu C, Clifford G D and Anderson D V 2017 Combining sparse coding and time-domain features for heart sound classification *Physiol. Meas.* **38** 1701
Winther S, Nissen L, Schmidt S E, Westra J, Andersen I T, Nyegaard M, Madsen L H, Knudsen L L, Urbonaviciene G and Larsen B S 2021 Advanced heart sound analysis as a new prognostic marker in stable coronary artery disease *European Heart Journal* **2** 279–89
Winther S, Nissen L, Schmidt S E, Westra J S, Rasmussen L D, Knudsen L L, Madsen L H, Johansen J K, Larsen B S and Struijk J J 2018 Diagnostic performance of an acoustic-based system for coronary artery disease risk stratification *Heart* **104** 928–35
Xiao S, Cai S and Liu G 2000 Studying the significance of cardiac contractility variability *IEEE Eng. Med. Biol. Mag.* **19** 102–5
Xu B, Kawata T, Daimon M, Kimura K, Nakao T, Lee S C, Hirokawa M, Yoshinaga A, Watanabe M and Yatomi Y 2018 Prognostic value of a simple echocardiographic parameter, the right ventricular systolic to diastolic duration ratio, in patients with advanced heart failure with non-ischemic dilated cardiomyopathy *Int. Heart J.* **59** 968–75
Yadav A, Singh A, Dutta M K and Travieso C M 2020 Machine learning-based classification of cardiac diseases from PCG recorded heart sounds *Neural Comput. Appl.* **32** 17843–56
Yamada M, Jitkrittum W, Sigal L, Xing E P and Sugiyama M 2014 High-dimensional feature selection by feature-wise kernelized lasso *Neural Comput.* **26** 185–207

Yancy C W, Jessup M, Bozkurt B, Butler J, Casey D E Jr, Colvin M M, Drazner M H, Filippatos G S, Fonarow G C and Givertz M M 2017 ACC/AHA/HFSA focused update of the 2013 ACCF/AHA guideline for the management of heart failure: a report of the american college of cardiology/American heart association task force on clinical practice guidelines and the heart failure society of America *J. Am. Coll. Cardiol.* **70** 776–803

Yeh J-R, Shieh J-S and Huang N E 2010 Complementary ensemble empirical mode decomposition: a novel noise enhanced data analysis method *Adv. Adaptive Data Anal.* **2** 135–56

Zhang W, Han J and Deng S 2017 Heart sound classification based on scaled spectrogram and tensor decomposition *Expert Syst. Appl.* **84** 220–31

Zheng Y and Guo X 2017 Identification of chronic heart failure using linear and nonlinear analysis of heart sound *2017 39th Annual Int. Conf. IEEE Engineering in Medicine and Biology Society (EMBC)* (IEEE) pp 4586–9

Zheng Y, Guo X, Jiang H and Zhou B 2017 An innovative multi-level singular value decomposition and compressed sensing based framework for noise removal from heart sounds *Biomed. Signal Process. Control* **38** 34–43

Zheng Y, Guo X, Qin J and Xiao S 2015 Computer-assisted diagnosis for chronic heart failure by the analysis of their cardiac reserve and heart sound characteristics *Comput. Methods Programs Biomed.* **122** 372–83